2012

Experimental and theoretical studies of hydroxyl-induced magnetism in TiO nanoclusters

Xiao-Hui Wei
University of Nebraska-Lincoln, sunshine@huskers.unl.edu

Rulong Zhou
University of Nebraska-Lincoln

Balamurugan Balamurugan
University of Nebraska-Lincoln, balamurugan@unl.edu

Ralph Skomski
University of Nebraska-Lincoln, rskomski2@unl.edu

Xiao Cheng Zeng
University of Nebraska-Lincoln, xzeng1@unl.edu

See next page for additional authors

Nanoscale

RSC Publishing

PAPER

Experimental and theoretical studies of hydroxyl-induced magnetism in TiO nanoclusters†

Cite this: *Nanoscale*, 2012, 4, 7704

Xiao-hui Wei,*[ac] Rulong Zhou,[c] B. Balamurugan,[ac] Ralph Skomski,[ac] Xiao Cheng Zeng*[bc] and D. J. Sellmyer*[ac]

A main challenge in understanding the defect ferromagnetism in dilute magnetic oxides is the direct experimental verification of the presence of a particular kind of defect and distinguishing its magnetic contributions from other defects. The magnetic effect of hydroxyls on TiO nanoclusters has been studied by measuring the evolution of the magnetic moment as a function of moisture exposure time, which increases the hydroxyl concentration. Our combined experiment and density-functional theory (DFT) calculations show that as dissociative water adsorption transforms oxygen vacancies into hydroxyls, the magnetic moment shows a significant increase. DFT calculations show that the magnetic moment created by hydroxyls arises from 3d orbitals of neighboring Ti sites predominantly from the top and second monolayers. The two nonequivalent hydroxyls contribute differently to the magnetic moment, which decreases as the separation of hydroxyls increases. This work illustrates the essential interplay among defect structure, local structural relaxation, charge redistribution, and magnetism. The microscopic differentiation and clarification of the specific roles of each kind of intrinsic defect is critical for the future applications of dilute magnetic oxides in spintronic or other multifunctional materials.

Received 21st September 2012
Accepted 11th October 2012

DOI: 10.1039/c2nr32858e

www.rsc.org/nanoscale

1 Introduction

Room-temperature ferromagnetism in dilute magnetic oxides (DMO) and dilute magnetic semiconductors (DMS) aroused enormous interest for potential applications in spintronics.[1,2] After more than a decade of intensive research, the origin of this ferromagnetism is still highly controversial. During the initial investigations of this defect ferromagnetism, efforts were centered on the roles of extrinsic defects such as dopants. The coexistence of dopants and cationic and anionic vacancies increases the difficulty of clarifying the role of each of them. Recent work is starting to focus on undoped metal oxides and the clarification of the specific role of each kind of intrinsic defect such as cationic and anionic vacancies. Two interesting cases are ZnS and ZnO nanostructures. DFT calculations for ZnS nanowires show that while S vacancy does not generate magnetic moments, Zn vacancies produce significant magnetic moments that scale with Zn vacancy concentration and arise from the 3p orbitals on neighboring S sites.[3] Similar DFT calculations for ZnO thin films and nanowires indicate that while O vacancies do not generate any magnetic moments, Zn vacancies give rise to magnetic moments that arise from the O 2p orbitals of neighboring O.[4] Both studies showcase the complex correlation among defect creation, local structural relaxation, charge redistribution, and magnetism. Another feature of the defect ferromagnetism is the preferential location of the vacancies at the surface of the nanostructures and these surface vacancies dominate the magnetic moment while interior vacancies give negligible contributions. Also the defect formation energy is reduced as the dimension of the sample is reduced from two-dimensional thin films to one-dimensional nanowires.[4] Thus nanostructures favor the defect ferromagnetism because of the higher surface area and defect concentration. The fact that oxygen vacancy (V_o) does not generate magnetic moments in ZnO can be attributed to the unique electronic structure of ZnO. As previous studies of various metal oxides point out, when the structure of a metal oxide becomes more complex, the bonding changes from ionic to covalent.[5,6] Thus while V_o generates defect states in simple oxides such as MgO and Al_2O_3, it does not for ZnO. Hence for many oxides, V_o is a crucial defect that affects the electronic structure and potentially gives rise to their room-temperature ferromagnetism.

Besides V_o, hydroxyl (OH) is another important defect that determines the physics and chemistry of metal oxides.[7–10] As a large number of metal oxides have comparable oxygen vacancy and hydroxyl concentrations, it is suggested that they share the same hydroxylation mechanism.[11] The (110) rutile TiO_2 surface

[a]*Department of Physics and Astronomy, University of Nebraska, Lincoln, Nebraska, 68588, USA*

[b]*Department of Chemistry, University of Nebraska, Lincoln, Nebraska, 68588, USA*

[c]*Nebraska Center for Materials and Nanoscience, University of Nebraska, Lincoln, Nebraska 68588, USA. E-mail: dsellmyer@unl.edu; sunshine@huskers.unl.edu; xzeng1@unl.edu*

† Electronic supplementary information (ESI) available: Fig. S1–S5. See DOI: 10.1039/c2nr32858e

has been used as a model system to investigate the hydroxylation process. Combined scanning tunneling microscopy (STM) and DFT calculations indicate that at each oxygen vacancy, a single water molecule is dissociated into an H atom and a hydroxyl. While the hydroxyl fills in the oxygen vacancy (V_o–OH), the H atom sits on a neighboring lattice O atom (H–O), effectively creating a nonequivalent hydroxyl pair (V_o–OH *vs.* H–O).[12,13] Moisture further facilitates the splitting of the hydroxyl pair, which is predominantly initiated by the diffusion of H–O, as well as the diffusion of the resulting single hydroxyls.[14] The diffusion energy barriers and attempt frequencies for each kind of hydroxyl also have been investigated. For TiO_2 containing 7% oxygen vacancies, the equilibrium hydroxyl separation is about 6 lattice spacings.[14] However the coexistent oxygen vacancy and hydroxyl are hard to differentiate since hydroxylation occurs even in ultra-high-vacuum conditions where only traces of moisture exist. Experimentally, electron-energy-loss spectroscopy fails to differentiate the two defects.[15] STM reveals a similar delocalization of electrons over multiple Ti atoms for the two defects except for slightly different electron-density shapes.[16] Enormous experimental and theoretical effort was also devoted to the distinction between oxygen vacancy and hydroxyl defects.

Oxygen vacancies and hydroxyls affect the electronic structure of titanium oxides differently giving rise to distinctive properties. For example, Au clusters adsorbed on TiO_2 surfaces with oxygen vacancies or hydroxyls show contrasting mobilities.[10] Hydrogenated anatase TiO_2 clusters show robust visible-light photocatalysis due to band-gap defect states.[17] DFT calculations for rutile TiO_2 show that both oxygen vacancies and hydroxyls create Ti^{3+} states in the band-gap and hydroxylation slightly stabilizes the energy.[18] Also the band-gap states for the latter are spin-polarized.[18] However, up to now, detailed electronic structure calculations to address the magnetic effect of hydroxyls and their distinction from oxygen vacancies have not been carried out, which is necessary to gain a thorough understanding of the room-temperature ferromagnetism in metal oxides considering the prevalence of the two defects.[19]

Direct experimental verification of the presence of a particular kind of defect and the distinguishing of its magnetic contribution from other coexistent defects is usually hard if not impossible to achieve. Defects in Ti oxides include Ti and O vacancies, Ti and O interstitials, hydroxyls, *etc.* In this work, we singled out the magnetic effect of hydroxyls by studying the evolution of the magnetic moment during hydroxylation, where oxygen vacancies are replaced by hydroxyls while other possibly coexistent defects are not affected. Micro-Raman studies further help to identify the presence of hydroxyls.

The study of clusters is advantageous because they enhance the surface-to-volume ratio which magnifies the surface effect. Of the various Ti oxides, TiO is especially interesting because of the highest defect concentration with spontaneous 15% vacancies on both the Ti and O sites.[20] This provides abundant adsorption sites for hydroxyls in the presence of moisture even at room temperature. Thus TiO is an ideal and convenient system to investigate the effect of hydroxyl defects on magnetism. Hydroxyls are introduced by exposing as-produced rock salt TiO clusters to moisture at room temperature, where hydroxylation occurs and V_o is replaced by OH.[12,13]

In this work, we perform detailed experiment and DFT calculations of the magnetic effect of the hydroxylation process on TiO nanoclusters. When these clusters are exposed to moisture, the magnetization displays a linear increase/exponential decay at increased/lowered humidity levels due to the adsorption/desorption of hydroxyls, respectively. Our micro-Raman spectroscopy shows direct evidence of the formation of single hydroxyls after moisture exposure as compared to the presence of only adsorbed moisture for as-produced TiO clusters. The creation of magnetic moments with hydroxyl adsorption is consistent with DFT calculations, which also reveal an intimate correlation among defect structure, local structural relaxation, charge redistribution, and magnetic moment. The magnetic moment is located at the surface, where the two nonequivalent hydroxyls contribute differently. Increasing the hydroxyl separation leads to decrease in magnetic moment.

2 Experimental methods

2.1 Fabrication of TiO_x clusters

The Ti oxide clusters are produced using inert-gas condensation in a cluster deposition system that has been described elsewhere[21] [ESI, Fig. S1†]. *In situ* and *ex situ* oxidations are used to obtain clusters of various composition and phases. *In situ* oxidation is realized by feeding oxygen into the condensation chamber, where various oxygen partial pressures lead to the formation of titanium monoxide and titanium dioxide of the anatase and rutile phases, respectively.[22] *Ex situ* oxidation is realized by annealing as-produced Ti clusters in oxygen, where the annealing temperature determines the composition and phases of the resulting oxide.[23] A representative TEM image of as-produced Ti clusters is shown in the [ESI, Fig. S2†]. For the TiO clusters, cluster films with total thicknesses of 150 nm and 40 nm are produced for comparative studies.

2.2 Characterization tools

Cluster size and film topography are examined with transmission-electron microscopy (TEM) and atomic-force microscopy (AFM), respectively. Magnetism is measured with a superconducting quantum interference device (SQUID). Raman spectroscopy is used to detect the presence of various hydroxyl and water species.

2.3 Manipulation of hydroxyl concentration and associated variation for the magnetization

To introduce hydroxyls, as-produced TiO cluster films are placed in a closed container filled with water vapor produced from water held at 350 K at atmospheric pressure. Magnetism is measured after each hour of storage in the moist-air container. Cluster films are examined after deposition and after 20 hours in moist air by Raman spectroscopy for the detection of hydroxyl groups.

After 15 hours of storage in the moist-air container, magnetic measurements indicate that an equilibrium state has been

reached. The moment relaxation is then studied. As ambient air has a lower humidity level than the moist air, hydroxyl desorption is expected. Similarly, oxygen annealing also leads to hydroxyl loss as well as V_o annihilation. Thus the moment relaxation is studied for both cases: during subsequent storage in ambient air and during oxygen annealing (at 450 °C). After oxygen annealing, moment recovery during re-exposure to ambient air is also studied.

3 Experimental results and discussion

3.1 Cluster size and film topography

As-produced TiO clusters are deposited onto carbon-coated Cu grid and Si substrate for TEM and AFM analyses, respectively. TEM image analysis yields an average size of 15 nm for the as-produced clusters [Fig. 1(a)]. AFM image analysis indicates that the root-mean-square thickness variation of the cluster film is 10 nm [Fig. 1(b)].

3.2 Evolution of magnetization during moisture exposure

The structure of the TiO cluster film is examined with XRD after deposition and after 20 hours of storage in moist air (Fig. 2). As-produced TiO clusters show the rock salt structure. After storage in moist-air, the rock salt structure and intensity ratios are maintained though the FWHM is slightly wider, presumably due to lattice distortion by adsorbed hydroxyls. Note that systematic lattice distortion can be induced by increasing hydroxyl densities.[24] A decrease of XRD intensity was also noticed for ZnO after hydrogen annealing.[25] It is well-known that hydrogen or vacuum annealing creates oxygen vacancies, which introduces hydroxyls subsequently.[26]

After each hour of storage in moist air, the hysteresis loop of the cluster film is measured at room temperature. For clarity, Fig. 3(a) shows only half of the hysteresis loops for a 150 nm thick TiO cluster film as a function of storage time in moist air. Representative whole hysteresis loops for storage durations of 0, 4, 10, 15 and 20 hours are shown in Fig. 3(b). It can be seen that the as-produced sample has a small diamagnetic signal. Storage in moist air transforms this signal to a ferromagnetic or ferromagnetic-like signal. As the moisture-exposure time increases, the magnetic moment increases and eventually reaches

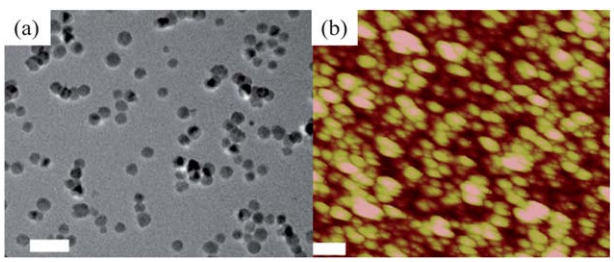

Fig. 1 Images of TiO clusters: (a) Examination of cluster size with transmission-electron microscopy. (b) Examination of the film topography with atomic-force microscopy. For TEM examination, as-produced TiO clusters are deposited on a copper grid. For AFM examination, a TiO cluster film is fabricated on a silicon substrate. The scales are 50 nm (TEM) and 100 nm (AFM), respectively.

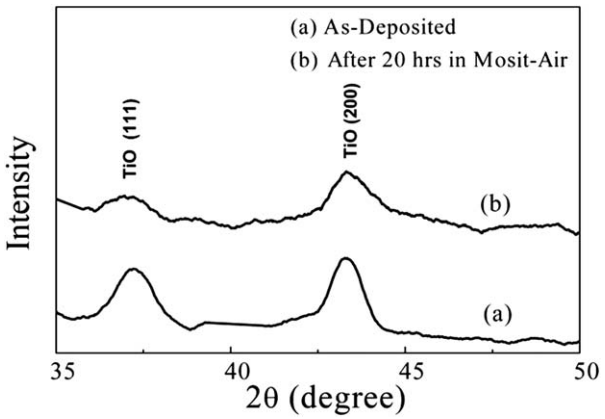

Fig. 2 Structural analysis of the TiO cluster film with X-ray diffraction: (a) after deposition and (b) after exposure to moisture at a temperature of 50 °C for 20 hours. The rock salt structure is maintained after moisture exposure.

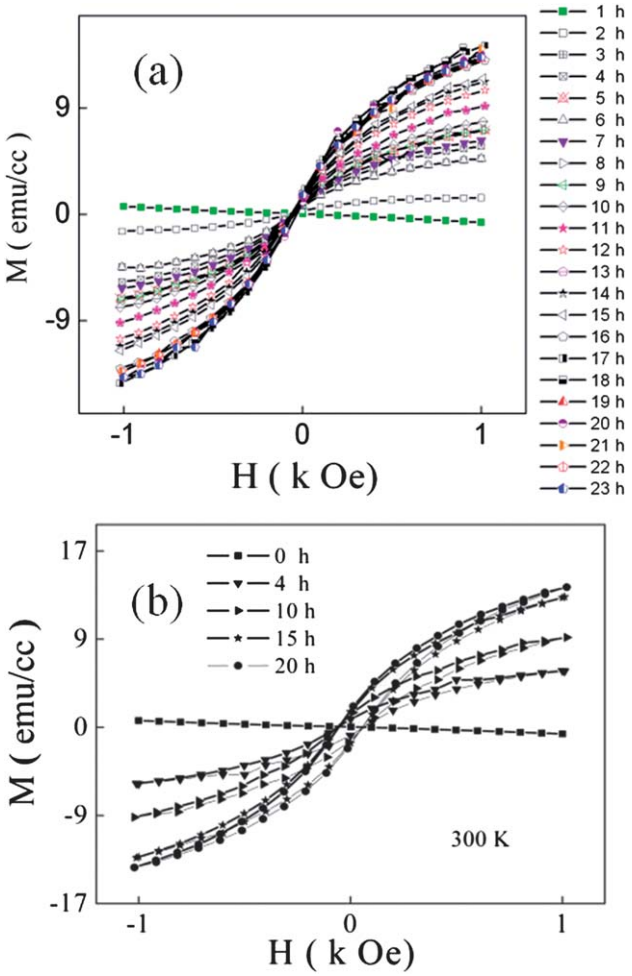

Fig. 3 Evolution of magnetism for the TiO cluster film during exposure to moisture examined with SQUID: (a) half hysteresis loops for the TiO cluster film, measured after each hour of storage in moist air. (b) Representative hysteresis loops for the TiO cluster film after different durations in moist air (0, 4, 10, 15 and 20 hours).

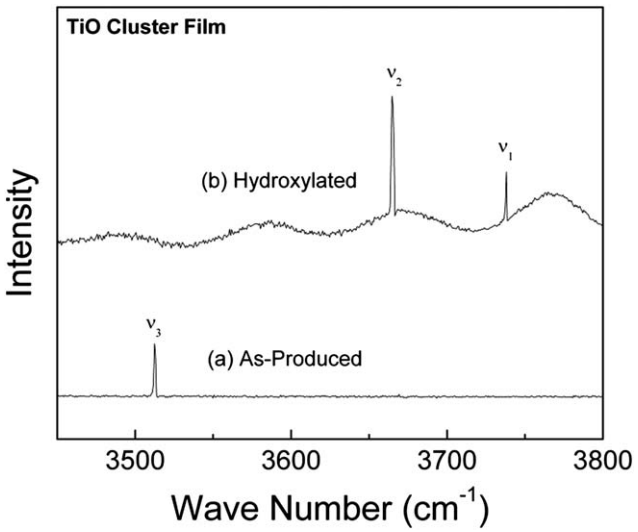

Fig. 4 Raman spectra of the TiO cluster film: (a) after deposition and (b) after 20 hours of storage in moist air. As-produced clusters show a single peak at 3512 cm^{-1} which can be attributed to adsorbed water. In contrast, after 20 hours of exposure to moisture, the Raman spectra of the cluster film show two peaks ν_1 at 3664 cm^{-1} and ν_2 at 3737 cm^{-1}, corresponding to the two nonequivalent hydroxyls.

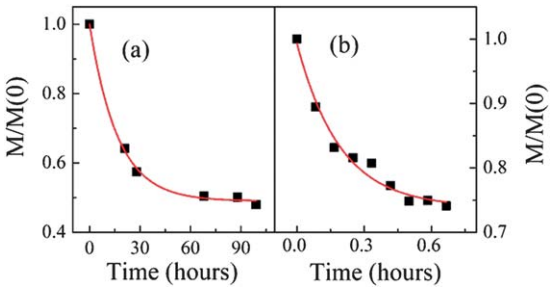

Fig. 5 Magnetization relaxation for a TiO cluster film (squares): (a) relaxation in ambient air after reaching equilibrium in moist-air. (b) Relaxation of the magnetization of the TiO cluster film during oxygen annealing at 450 °C after reaching the equilibrium value in moist air. Solid lines are exponential fits.

equilibrium after 17 hours with a magnetization of 13.5 emu cm^{-3} and a coercivity of 70 Oe. After the magnetization reaches equilibrium during moisture exposure, if all V_o are replaced by hydroxyls, each pair of hydroxyls will correspond to a moment of 3.5μ_B per pair at a hydroxyl separation of 1.29 lattice spacing. Note that the calculation has assumed that the TiO clusters have the same oxygen vacancy concentration as the bulk, *i.e.* 15 at.%. As the oxygen vacancy concentration can be affected by fabrication conditions such as the oxygen partial pressure, this value serves only as a rough estimation of the moment.

To detect hydroxyls, the TiO cluster film is examined with Raman spectroscopy after deposition [Fig. 4(a)] and after 20 hours of moisture exposure [Fig. 4(b)]. As-produced clusters show a single peak at 3512 cm^{-1}, which likely arises from adsorbed moisture.[24,27,28] In contrast, after 20 hours of moisture exposure, the Raman spectrum of the cluster film shows two peaks at 3664 cm^{-1} and 3737 cm^{-1}, which likely arise from the two nonequivalent hydroxyls.[27]

This assignment of the Raman peak in the as-produced sample to adsorbed moisture/newly created hydroxyl pair and the Raman peaks in an aged sample to single hydroxyls is logical, reflecting the creation of single hydroxyls after moisture adsorption.

After the moment reaches equilibrium in moist air, its relaxation is studied in both ambient air [Fig. 5(a)] and during oxygen annealing [Fig. 5(b)]. Interestingly for both cases, exponential relaxations are observed. Distinctive time constants of 16 days and 19 minutes are obtained, reflecting the higher rate of hydroxyl loss during annealing. After the oxygen annealing, moment recovery during re-exposure to moist and ambient air is investigated. The magnetic moment does not increase quickly in moist air as in the as-produced sample, probably due to the annihilation of oxygen vacancies and modification of the structure by annealing.

3.3 Comparative study of the aging behaviors of TiO and TiO_2 clusters

We also have performed a comparative study of the aging behaviors of Ti monoxide and dioxide clusters in ambient air. The TiO clusters have a much higher moment increase rate and saturation value than the dioxide clusters [ESI, Fig. S3†]. After storage in ambient air for 1 month, the TiO cluster film develops a magnetization of 12 emu cm^{-3}. However, after one year, the anatase and rutile TiO_2 cluster films reveal magnetizations of 0.4 emu cm^{-3} and 0.3 emu cm^{-3}, respectively. Note that the moment increase rate is affected by various factors such as the oxygen vacancy concentration, the diffusion rate of hydroxyls, as well as the specific structure of the oxide. The relative stability of the magnetic moment is also investigated. The magnetic moment of titanium monoxide shows much higher stability than the dioxides. While the moment of the TiO clusters is stable over a range of two years, the moment of the anatase and rutile TiO_2 clusters disappears after one year. Note that the oxygen vacancy or associated hydroxyl densities for TiO, anatase and rutile TiO_2 are in the order of TiO > anatase TiO_2 > rutile TiO_2, which likely explains the different increase rates, saturation values, and the stabilities of the magnetic moments.[28]

3.4 Summary of experimental results

A schematic diagram of moisture-induced hydroxylation and magnetic moment in TiO clusters is shown in Fig. 6(a). As-produced TiO clusters have abundant oxygen vacancies. Upon exposure to moisture, water molecules adsorb at oxygen vacancies and create hydroxyls. As hydroxylation progresses with further water adsorption, the magnetic moment increases with the hydroxyl density. Fig. 6(b) shows the magnetization as a function of storage time in moist air, where it increases approximately linearly before reaching the equilibrium state. This behavior is also observed in the thinner sample (40 nm thick) [ESI, Fig. S4†], indicating that the magnetic moment is not restricted to the surface of the cluster film; instead, the whole cluster film has a homogeneous contribution to the magnetization. Since ambient air contains less moisture compared to moist air, we expect this behavior to occur in ambient air at a lower rate. Actually, it took 1 month for the

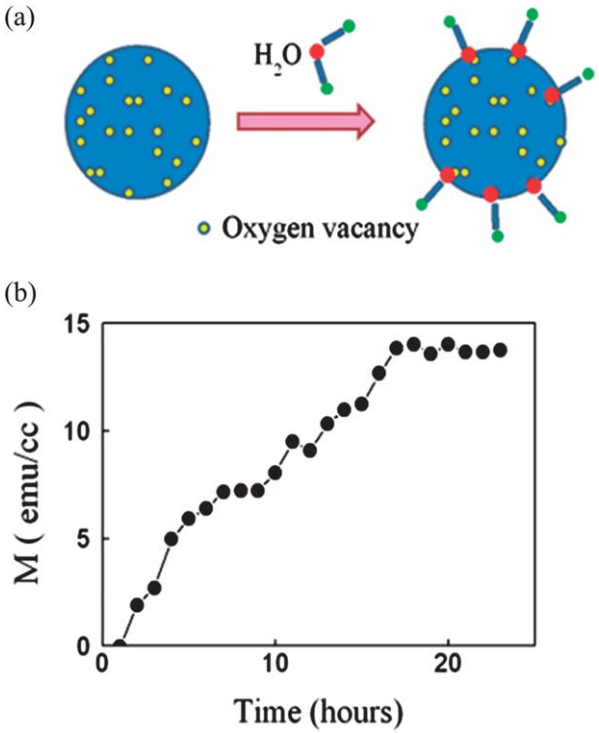

Fig. 6 (a) Schematic diagram of hydroxyl creation at oxygen vacancies in a TiO cluster during moisture exposure. (b) Evolution of the magnetization as a function of storage time in moist air.

magnetic moment to reach the equilibrium value thanks to the lower humidity level and concentration of water molecules.

3.5 Discussion

Previous investigation of the temperature-dependent conductivity of oxides containing both oxygen vacancy and hydroxyls shows that the conductivity is controlled by diffusion of both.[24] Below 200 °C, hydroxyl diffusion dominates while above 200 °C both oxygen vacancy and hydroxyl diffusion are involved.[24] Note that the conductivity of various metal oxides also show linear increase/exponential decay at higher/lower humidity levels similar to the variation of the magnetic moment here.[29,30] The common underlying reason is probably the increased/decreased hydroxyl concentrations at elevated/decreased humidity levels, respectively. Saturation of hydroxyls likely gives rise to the moment saturation.[31] Each oxygen vacancy introduces a pair of hydroxyls which doubles the defect concentration. As a single oxygen vacancy and a single hydroxyl generate similar electron delocalization over multiple proximate Ti atoms, the conductivity increase is likely due to the enhanced charge delocalization with doubled defect density induced by hydroxylation. This correlation between conductivity and ferromagnetism is consistent with previous suggestions of carrier-mediated ferromagnetism.[2]

The presence of oxygen vacancies and hydroxyls in other metal oxides and the comparable magnetizations reported for many of them suggest that the hydroxyl-induced magnetic moment might also be true for other metal oxides. Experimental methods that modify oxygen vacancy and hydroxyl concentrations also produce significant variations of the magnetism. Moment enhancement has been frequently reported for a variety of metal oxides after vacuum or hydrogen annealing, which is known to introduce oxygen vacancies and subsequently hydroxyls. The magnetizations of TiO_2 and HfO_2 thin films also display exponential decays during oxygen annealing [ESI, Fig. S5†]. Previously, for In_2O_3, the carrier density was found to have a stretched exponential decay during storage in air.[32] A power-law decay is reported for the magnetic moment of ZnO during storage in air.[33] It is suggested that these relaxations can be ascribed to Arrhenius type behavior with a distribution of diffusion-site energies.[34] Detailed electronic structure calculations are still necessary to clarify the role of hydroxyls for a particular oxide.

4 DFT calculations

4.1 Guidelines for calculation

DFT calculations are performed to clarify the origin of the hydroxyl-induced magnetic moment. The following issues are considered: (i) dependence of H adsorption on the defect structure. In this case, three different environments are considered: (1) perfect TiO; (2) TiO with only V_o; and (3) TiO with coexistent V_o and V_{Ti}. (ii) Differentiation of the magnetic roles of the two nonequivalent hydroxyls (V_o–OH *vs.* H–O). (iii) The spatial location of the magnetic moment: on the surface *vs.* in the interior. Previous DFT calculations for anatase TiO_2 indicate that V_o creates band-gap states, the width of which scales with the V_o density.[10] Thus we have also investigated the effect of oxygen vacancy density, for which one and two V_o in one supercell are considered, respectively. (iv) Long-term stability of the magnetic moment, or in effect moment–energy correlation. Correlation between magnetism and hydroxyl separation are examined.

All the DFT calculations are performed with a plane-wave basis set as implemented in the VASP package. An energy cutoff of 400 eV and the Perdew–Burke–Ernzerh of GGA exchange and correlation functional are adopted. A slab containing 6 atomic layers along the *c* axis and (3 × 3) unit cells in the *x*–*y* planes is selected as the model of the TiO (110) surface. The atoms in the bottom two layers are fixed during the structural relaxations. A

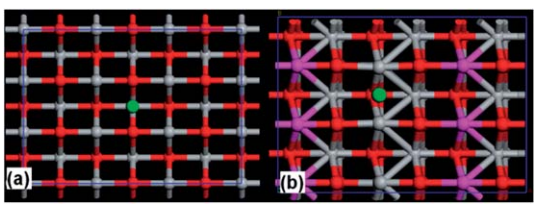

Fig. 7 DFT calculation results for H adsorption on the surface of a perfect TiO (110) nanocrystal. (a) H adsorption before relaxation, where H is attached to the bridging site between two O atoms. (b) H adsorption after structural relaxation, where the H atom has moved to the bridging site between two Ti atoms. H, Ti and O atoms are designated by green, gray and red/pink spheres, respectively. For the relaxed structure, Ti atoms that show magnetic moments are designated by pink in (b).

uniform 8 × 8 × 1 *k*-point mesh sampled with the Monkhorst–Pack scheme is selected during all the surface calculations. For the bulk solid calculation, the supercell contains 2 × 2 × 2 unit cells. The Brillouin zone is sampled with an 8 × 8 × 8 grid.

4.2 H adsorption on a perfect TiO surface

First, we consider H adsorption on the perfect surface. Three adsorption sites are considered: on top of O atom, the bridging site between two O atoms, and the bridging site between one O and one Ti atom. Before structural relaxation, H is located at the bridging site between two O atoms. After structural relaxation, the H atom moves to the bridging site between two Ti atoms [Fig. 7]. The adsorption energy in this case (defined as $E_a = -(E_{tot} - E_{surf} - E_H)$) is 8.25 eV. The total energies of the other two cases are about 1.9 eV (adsorbed on O) and 1.4 eV (adsorbed between O and Ti) higher, respectively. Such large energy differences indicate that the bridging site between two Ti atoms (after relaxation) is energetically the most favorable. With H adsorption, the total magnetic moment increases by about $6\mu_B$. This arises from the significant increase of the magnetic moments for Ti atoms located in the two neighboring Ti rows (Fig. 7(b), pink). To conclude, both the magnetic moment and H adsorption depend sensitively on the structural relaxation.

4.3 H adsorption on a TiO surface with only oxygen vacancies

We have further examined H adsorption in the presence of V_o. Different Ti and O adsorption sites near the O vacancy are considered. The most favored Ti sites and O site for H adsorption are as shown in Fig. 8(a). H adsorption on Ti-sites is more stable than that on O sites (2.2 eV lower in total energy). H adsorption on Ti_{site1} and Ti_{site2} has comparable adsorption energies. The case of H adsorption on Ti_{site1} is shown in Fig. 8(b). Thus, on the TiO(110) surface with only V_o defects, when a single H atom is deposited near a single O vacancy, it will be adsorbed on Ti-sites, resulting in small total magnetic moments ($1.1\mu_B$ and $0.2\mu_B$ for Ti_{site1} and Ti_{site2} respectively). We also examined moment generation by V_o in the interior of the TiO crystal as well as the effect of V_o concentration. For all cases, no magnetic moment is detected with or without H adsorption.

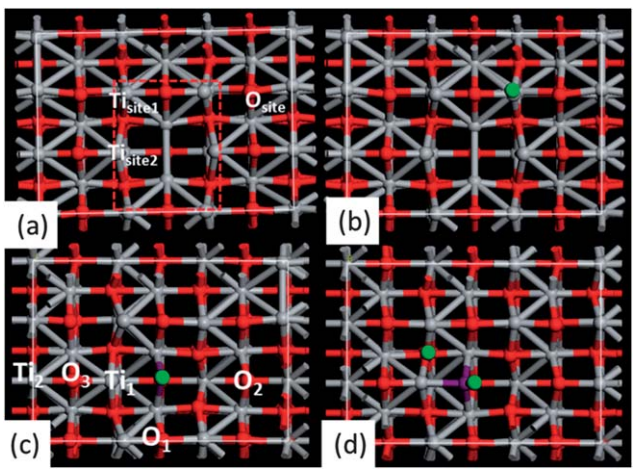

Fig. 8 DFT calculation results for H adsorption on the (110) surface of a defective TiO nanocrystal: (a) relaxed (110) surface of a TiO nanocrystal with only V_o; the multiple H adsorption sites considered in the calculations are also shown. (b) The most stable H adsorption site (Ti_{site1}) after structural relaxation for a TiO (110) surface with only V_o. (c) Adsorption of OH on V_o of a TiO (110) surface with coexistent V_{Ti} and V_o. (d) Second H adsorption in addition to V_o–OH on a relaxed TiO (110) surface with coexistent V_{Ti} and V_o. H atoms are designated by green balls and are positioned at the most stable adsorption sites.

4.4 OH adsorption on a TiO surface with coexisting Ti and O vacancies

We first considered the magnetism of a TiO(110) surface with coexistant V_{Ti} and V_o. Out of the various V_{Ti}–V_o configurations, the most stable V_{Ti}–V_o complex exhibits a magnetic moment of $2.6\mu_B$.

We then considered the magnetism when a single hydroxyl is adsorbed at an oxygen vacancy. When an OH fills in the O vacancy [Fig. 8(c)], the total magnetic moment jumps to $9.3\mu_B$. While O and H atoms give rise to little magnetic moment, Ti atoms from neighboring Ti rows in the utmost top layer and the sub-monolayer dictate the magnetism. From the surface to the interior, the contribution decreases rapidly. Comparatively, Ti atoms in the top layer have higher moments that vary from 0.3 to $0.6\mu_B$/Ti, while Ti atoms from the sub-monolayer have relatively smaller moments of about $0.1\mu_B$/Ti. For both the top layer and the sub-monolayer, the intra-layer couplings between Ti atoms are ferromagnetic. However, the interlayer coupling, the coupling between the top and the sub-monolayer, is antiferromagnetic. The contrasting coupling for the interlayer and the intralayer might be due to the significantly different interatomic separations between Ti atoms. Note that the interatomic distance between Ti atoms in the top layer as well as that of the sub-monolayer are about 3 A. However, the interlayer separation is much smaller, which is about 2.66 A.

As a single water molecule dissociatively adsorbs at a V_o, a pair of nonequivalent hydroxyls are generated on neighboring sites. As the hydroxyl pair splits up and the resultant single hydroxyls diffuse away, the separation of the two non-equivalent hydroxyls increases over time. The evolution of the magnetic moment as a function of the hydroxyl separation is thus worthy of consideration. We first examined the magnetic moment of a freshly created hydroxyl pair, which is realized by adding one more H to a neighboring O next to the V_o–OH [Fig. 8(d)]. As experiments show, after the geminated hydroxyl pair is created upon dissociative water adsorption, moisture further facilitates the splitting and diffusion of the resultant single hydroxyls, a process which is dominated by the diffusion of the hydroxyls involving one lattice O (H–O).[14] Thus we examined the energetics of this splitting and diffusion process. This is realized by analyzing the relative stabilities of the additional H adsorption on different O and Ti sites with various separations from the other hydroxyls (V_o–OH). Three different O sites and two Ti sites are considered. Of the various O adsorption sites, H adsorption to O2 is the most stable, for which the adsorption energy is lower than that of O1 and O3 by 0.11 eV and 0.49 eV, respectively. The total magnetic moment scales with the separation between the two nonequivalent

hydroxyls: H–O and V_o–OH. H adsorption next to the V_o–OH gives the highest moment ($O_1/13\mu_B$), which decreases as H diffuses away ($O2/10\mu_B$, $O3/4.9\mu_B$). In the long term, energy stabilization leads to diffusion of newly formed hydroxyls to adsorption sites with both lower energy and moment, resulting in dwindling of the magnetic moment consistent with experimental observations of moment relaxation.

To determine the location of the magnetic moment, we also examined defects located in the interior of the TiO crystal. For this case, no magnetic moment is detected with or without H adsorption near the defects. Thus, the magnetic moments of TiO clusters mainly originate from the cluster surface instead of the bulk.

4.5 Summary of DFT calculations

In summary, our DFT calculations suggest an intimate correlation between the defect structure and the magnetism. H adsorption sensitively depends on the structural relaxation unique to each defect structure. Coexistence of V_o and V_{Ti} is essential to reproduce the creation of magnetic moment with hydroxyl adsorption. This is consistent with the normal experimental observation of coexistent Ti and O vacancies in TiO. Of the two nonequivalent hydroxyls, V_o–OH contributes predominantly to the magnetism. The magnetic moment is restricted to the cluster surface. The coupling sensitively depends on the interatomic separation, illustrating the crucial role of structural relaxation. In the long term, stabilization of the system leads to diffusion of hydroxyls to adsorption sites with both lower energies and lower moments, leading to the eventual dwindling and disappearance of the magnetic moment. The hydroxyl-induced magnetism in our anatase and rutile TiO_2 clusters provides experimental evidence for previous DFT calculations of spin-polarized bandgap states for hydroxylated and reduced TiO_2 surfaces.[19]

Our DFT calculations show the microscopic creation of magnetic moment upon hydroxyl adsorption. Experimentally, we observe the overall macroscopic feature. When as-produced TiO clusters are exposed to moisture, the magnetic moment increases linearly and subsequently reaches saturation. Previous STM investigation of transition metal oxide surface indicates that the surface hydroxyl coverage displays a roughly linear increase before reaching saturation.[35] Thus the linear increase and subsequent saturation behavior of the magnetic moment can be correlated with the identical variation of the hydroxyl density. As the conductivity of metal oxides also displays a linear increase during water exposure, it is reasonable to correlate the hydroxyl density, conductivity, and the magnetic moment, consistent with the notion of carrier-mediated ferromagnetism.[2]

The calculated total magnetic moment of a hydroxyl pair decreases with increasing separation and reaches a value of $5\mu_B$ per pair at a separation of one lattice spacing. The lower magnetic moment observed experimentally, $3.5\mu_B$ per pair at a hydroxyl separation of 1.29 lattice spacing, may arise from the bigger separation between hydroxyls, consistent with the decaying of magnetic moment with increasing hydroxyl separation from DFT calculations.

As to the moment of oxygen vacancy, assuming that the moment of the as-produced sample is mainly from oxygen vacancies, neglecting the minimal contamination with adsorbed water and resultant hydroxyl pairs from the deposition chamber, the moment of each oxygen vacancy can be estimated to be at least one order of magnitude smaller than that of hydroxyls.

To clarify the origin of the defect ferromagnetism in DMS and DMO, the roles of intrinsic defects, such as cationic and anionic vacancies, and extrinsic defects such as dopants are extensively examined. Recent works specifically have addressed the role of each kind of defect in undoped oxides. Though these works concern different DMO and DMS systems, they share several similarities to our TiO clusters: (i) the magnetic moment does not reside on the defect, instead it arises from neighboring sites. For ZnS nanowires, the moment is located on neighboring S sites around Zn vacancies and arises from S 3p orbitals.[3] For TiO nanoclusters, the moment originates from neighboring Ti atoms surrounding oxygen vacancies and arises from Ti 3d orbitals. For ZnO nanowires, the moment is located on neighboring O sites and arises from O 2p orbitals.[4] All share a complicated correlation among defect structure, structural relaxation, charge delocalization, and magnetism. (ii) The moment is predominantly located at the surface of the nanostructures, which involves the first few monolayers where the contribution dwindles quickly from the surface to the interior. (iii) The moment generated by each defect is of the same order of magnitude, about a few μ_B. (iv) The total moment scales with the defect density. As representative DMO and DMS systems, these works point out the necessity of differentiating various kinds of defects, which create specific structural relaxations, associated charge delocalizations, and magnetism. The intrinsic defect induced ferromagnetism in DMO and DMS is more favorable than transition-metal doping for applications in biomedicine as transition metals can form dangerous free radicals.

The humidity-sensitive magnetism in TiO clusters is in striking similarity to that of molecular magnets such as Prussian blue analog.[36–41] Adsorption/desorption of hydroxyls produces the moment variation for our Ti oxide clusters. Adsorption/desorption of water molecules give rise to the moment variation for molecular magnets.[36–41] Both systems display intimate correlations among defect structure, humidity, conductivity, and magnetism, highlighting the crucial and promising role of defect-engineering in new material development.

5 Conclusions

The magnetic moment of as-produced TiO clusters exhibits linear increase/exponential relaxation due to the adsorption/desorption of hydroxyls, respectively. DFT calculations show that with coexistent O and Ti vacancies, hydroxyl adsorption at oxygen vacancies generates significant magnetic moments, which reside on neighboring Ti sites and arise from the Ti 3d orbitals. These moments are predominantly located at the surface and decrease as the hydroxyl separation increases, which reflect the correlation between energy stabilization and relaxation of the magnetism. As many metal oxides share comparable hydroxyl densities, hydroxyl-induced magnetic

moments may also play a role, which needs verification with detailed electronic structure calculations. The humidity sensitivity and the correlation among defect structure, conductivity, and magnetism suggests applications in H or moisture sensors, molecule detection, spintronics, photocatalysis, fuel cells, and other multifunctional materials.[40–42]

Acknowledgements

We thank Professor Yongfeng Lu for use of the Raman spectroscopy equipment. This research is supported by NSF-MRSEC (DMR 0820521) [XHW, RZ, RS], ARO (W911NF-10-2-0099) [BB, XCZ, DJS], and NCMN facilities. Computing support from UNL Holland Computing Center and from Center for Functional Nanomaterials in Brookhaven National Laboratory is highly appreciated.

Notes and references

1 T. Dietl, *Nat. Mater.*, 2010, **9**, 965.
2 J. M. D. Coey and S. A. Chambers, *MRS Bull.*, 2008, **33**, 1053.
3 G. Zhu, S. Zhang, Z. Xu, J. Ma and X. Shen, *J. Am. Chem. Soc.*, 2011, **133**, 15605.
4 Q. Wang, Q. Sun, G. Chen, Y. Kawazoe and P. Jena, *Phys. Rev. B: Condens. Matter Mater. Phys.*, 2008, **77**, 205411.
5 J. Carrasco, N. Lopez and F. Illas, *Phys. Rev. Lett.*, 2004, **93**, 225502.
6 R. D. Parra and H. H. Farrell, *J. Phys. Chem. C*, 2009, **113**, 4786.
7 S. Li, L. Chu, X. Gong and U. Diebold, *Science*, 2010, **328**, 882.
8 K. Onda, B. Li, J. Zhao, K. D. Jordan, J. Yang and H. Petek, *Science*, 2005, **308**, 1154.
9 I. Justicia, P. Ordejón, G. Canto, J. L. Mozos, J. Fraxedas, G. A. Battiston, R. Gerbasi and A. Figueras, *Adv. Mater.*, 2002, **14**, 1399.
10 D. Matthey, J. G. Wang, S. Wendt, J. Matthiesen, R. Schaub, E. Lægsgaard, B. Hammer and F. Besenbacher, *Science*, 2007, **315**, 1692.
11 H. Tamura, K. Mita, A. Tanaka and M. Ito, *J. Colloid Interface Sci.*, 2001, **243**, 202.
12 R. Schaub, P. Thostrup, N. Lopez, E. Lægsgaard, I. Stensgaard, J. K. Nørskov and F. Besenbacher, *Phys. Rev. Lett.*, 2001, **87**, 266104.
13 S. Wendt, J. Matthiesen, R. Schaub, E. K. Vestergaard, E. Lægsgaard, F. Besenbacher and B. Hammer, *Phys. Rev. Lett.*, 2006, **96**, 066107.
14 S. Li, Z. Zhang, D. Sheppard, B. D. Kay, J. M. White, Y. Du, I. Lyubinetsky, G. Henkelman and Z. Dohnálek, *J. Am. Chem. Soc.*, 2008, **130**, 9080.
15 M. A. Henderson, W. S. Epling, C. H. F. Peden and C. L. Perkins, *J. Phys. Chem. B*, 2003, **107**, 534.
16 T. Minato, Y. Sainoo, Y. Kim, H. S. Kato, K. Aika, M. Kawai, J. Zhao, H. Petek, T. Huang, W. He, B. Wang, Z. Wang, Y. Zhao, J. Yang and J. G. Hou, *J. Chem. Phys.*, 2009, **130**, 124502.
17 X. Chen, L. Lu, P. Y. Yu and S. S. Mao, *Science*, 2011, **331**, 746.
18 C. Di Valentin, G. Pacchioni and A. Selloni, *Phys. Rev. Lett.*, 2006, **97**, 166803.
19 R. Skomski, X. Wei, B. Balamurugan, M. Chipara and D. J. Sellmyer, *IEEE Trans. Magn.*, 2010, **46**, 2427.
20 A. F. Wells, *Structural Inorganic Chemistry*, Clarendon, Oxford, UK, 1975.
21 Y. F. Xu, M. L. Yan and D. J. Sellmyer, in *Advanced Magnetic Nanostructures*, ed. D. J. Sellmyer and R. Skomski Springer, New York, 2006, Ch. 8, p. 207.
22 B. Balasubramanian, K. L. Kraemer, N. A. Reding, R. Skomski, S. Ducharme and D. J. Sellmyer, *ACS Nano*, 2010, **4**, 1893.
23 X. Wei, R. Skomski and D. J. Sellmyer, *IEEE Trans. Magn.*, 2009, **45**, 4089.
24 H. Jena, K. V. G. Kutty and T. R. N. Kutty, *Mater. Res. Bull.*, 2004, **39**, 489.
25 W. M. Hlaing Oo, M. D. McCluskey, J. Huso and L. Bergman, *J. Appl. Phys.*, 2007, **102**, 043529.
26 Q. Zhao, P. Wu, B. L. Li, Z. M. Lu and E. Y. Jiang, *J. Appl. Phys.*, 2008, **104**, 073911.
27 K. S. Finnie, D. J. Cassidy, J. R. Bartlett and J. L. Woolfrey, *Langmuir*, 2001, **17**, 816.
28 S. Shoval, S. Yariv, K. H. Michaelian, M. Boudeulle and G. Panczer, *Clays Clay Miner.*, 2002, **50**, 56.
29 G. Wang, Q. Wang, W. Lu and J. Li, *J. Phys. Chem. B*, 2006, **110**, 22029.
30 F. Hernandez-Ramirez, S. Barth, A. Tarancon, O. Casals, E. Pellicer, J. Rodriguez, A. Romano-Rodriguez, J. R. Morante and S. Mathur, *Nanotechnology*, 2007, **18**, 24016.
31 S. Yamamoto, H. Bluhm, K. Andersson, G. Ketteler, H. Ogasawara, M. Salmeron and A. Nilsson, *J. Phys.: Condens. Matter*, 2008, **20**, 184025.
32 R. Dixit, P. Panguluri, C. Sudakar, P. Kharel, P. Thapa, I. Avrutsky, R. Naik, G. Lawes and B. Nadgorny, *Appl. Phys. Lett.*, 2009, **94**, 252105.
33 A. Zukova, S. Teiserskis, Y. K. Dijken Gun'ko and V. Kazlauskiene, *Appl. Phys. Lett.*, 2004, **89**, 232503.
34 J. Kakalios, R. A. Street and W. B. Jackson, *Phys. Rev. Lett.*, 1987, **59**, 1037.
35 G. S. Parkinson, Z. Novotný, P. Jacobson, M. Schmid and U. Diebold, *J. Am. Chem. Soc.*, 2011, **133**, 12650.
36 S. Ohkoshi, K. Nakagawa, K. Tomono, K. Imoto, Y. Tsunobuchi and H. Tokoro, *J. Am. Chem. Soc.*, 2010, **132**, 6620.
37 H. Okawa, A. Shigematsu, M. Sasakiyo, T. Miyagawa, K. Yoneda, M. Ohba and H. Kitagawa, *J. Am. Chem. Soc.*, 2009, **131**, 13516.
38 C. Cartier dit Moulin, F. Villain, A. Bleuzen, M. Arrio, P. Sainctavit, C. Lomenech, V. Escax, F. Baudelet, E. Dartyge, J. Gallet and M. Verdaguer, *J. Am. Chem. Soc.*, 2000, **122**, 6653.
39 E. Coronado, J. R. Galan-Mascaros, C. J. Gomez-Garcia and V. Laukhin, *Nature*, 2000, **408**, 447.
40 M. Sadakiyo, T. Yamada and H. Kitagawa, *J. Am. Chem. Soc.*, 2009, **131**, 9906.
41 S. Ohkoshi, K. Arai, Y. Sato and K. Hashimoto, *Nat. Mater.*, 2004, **3**, 857.
42 O. Sato, T. Iyoda, A. Fujishima and K. Hashimoto, *Science*, 1996, **272**, 704.